Electrochemical Conversion of Oxide Precursors to Consolidated Zr and Zr−2.5Nb Tubes

Junjun Peng,[†] Kai Jiang,[†] Wei Xiao,[†] Dihua Wang,*[,†] Xianbo Jin,[†] and George Z. Chen*[,†,‡]

College of Chemistry and Molecular Sciences, Wuhan University, Wuhan, 430072, P.R. China, and Department of Chemical and Environmental Engineering, Faculty of Engineering, University of Nottingham, Nottingham, NG7 2RD, United Kingdom

Received August 18, 2008. Revised Manuscript Received October 7, 2008

Porous tubular oxide precursors have been fabricated from the ZrO_2 powder and its mixture with the Nb_2O_5 powder, and directly metallised to pure Zr or the Zr−2.5Nb Zircaloy tubes through electrochemical reduction and deoxygenation that induces in situ consolidation or sintering of the metallized tubes in molten $CaCl_2$ at ~900 °C. This new process is simple, fast, and low in energy consumption, promising a new technology for the fabrication of zirconium/Zircaloy tubes, which are the crucial materials in nuclear reactors and chemical plants. Also reported in this paper is the mechanism of the electrochemical process, correlating the cyclic voltammogram of ZrO_2 powder in a metallic cavity electrode with the morphological and compositional analyses of the products from potentiostatic electrolysis of porous ZrO_2 pellets.

Introduction

Zirconium (Zr) has a small neutron absorption cross-section and is also mechanically strong and corrosion-resistant. This unique combination of properties leads to more than 90% of the Zr metal produced in the world being used in the fuel cladding tubes in various nuclear reactors.[1−5] In the current industry, however, the cladding tubes are manufactured through a long process of multiple steps, including (1) conversion of the mineral (e.g., zircon, $ZrSiO_4$, and baddeleyite, ZrO_2) to $ZrCl_4$ via carbochlorination ($ZrSiO_4 + 4Cl_2 + 4C = ZrCl_4 + SiCl_4 + 4CO$), (2) magnesiothermic reduction of the vaporised $ZrCl_4$ to the Zr metal sponge (i.e., the Kroll process, $ZrCl_4 + 2Mg = Zr + 2MgCl_2$), (3) alloy production by electric-arc melting the Zr sponge with other metals to the needed composition (e.g., Zircaloy, mainly Zr−Sn−Nb-etc.), and (4) multistep fabrication of the alloy into the cladding tubes (e.g., forging, extrusion, rolling, and/or annealing).[6−14] In fact, such multistep processes are commonly used for manufacturing many other metallic artifacts.

It was recently reported that ZrO_2 could be directly converted to the Zr metal[15−18] via two different approaches: metallothermic reduction[19,20] and electrochemical reduction[21−34] in molten salts. In the electrochemical process, the powder of pure or mixed oxides is made into a porous cathode and then electrolyzed in a molten salt (e.g., $CaCl_2$ or LiCl) in conjunction with an graphite or inert anode. The

* Corresponding author/ Tel: 44 (0)115 9514171 (G.Z.C.); 86(0)27 68775799 (D. H.W.). Fax: 44 (0)115 9514115 (G.Z.C.); 86(0)27 68756319 (D. H.W.). E-mail: george.chen@nottingham.ac.uk (G.Z.C.); wangdh@whu.edu.cn (D. H.W.).

[†] Wuhan University.

[‡] University of Nottingham.

(1) Adamson, R. B.; Van Swam L. F. P., Eds.; *Zirconium in the Nuclear Industry: Seventh International Symposium*; ASTM: Philadelphia, PA, 1987.
(2) Aymovsky, A. C. *Zirconium Alloys for Nuclear Power*; translated from Russian by. Yao, M. Z.; Atomic Energy Press of China: Beijing, 1988; in Chinese.
(3) Gamboges, J. Zirconium and Hafnium. *2005 Minerals Yearbook*; U.S. Geological Survey: Reston, VA, 2005.
(4) http://www.speclab.com/elements/zirconium.htm.
(5) http://minerals.usgs.gov/minerals/pubs/commodity/zirconium/730798.pdf.
(6) Farhat, Z. N. *Mater. Sci. Eng., A* **2007**, *474*, 96.
(7) Hong, S. I.; Lee, K. W. *J. Nucl. Mater.* **2005**, *340*, 203.
(8) Findlay, R. G. U.S. Patent US2828201, 1958.
(9) Ishimatsu, K.; Nakahara, T. U.S. Patent US3692294, 1971.
(10) Isobe, T.; Mural, T. European Patent EP1223587, 2002.
(11) Sabol, G. P.; McDonald, S. G. U.S. Patent US4649023, 1987.
(12) Une, K.; Ishimoto, S. *J. Nucl. Mater.* **2003**, *323*, 101.
(13) Vizcaíno, P.; Banchik, A. D.; Abriata, J. P. *J. Nucl. Mater.* **2002**, *304*, 96.
(14) Khatamian, D.; Shaddick, A. *J. Alloys Compd.* **1999**, *324*, 293.
(15) Chen, G. Z.; Fray, D. J. *Light Met.* **2001**, 1147.
(16) Abdelkader, A. M.; Daher, A. R.; Abdelkareem, A.; El-Kashif, E. *Metall. Mater. Trans. B* **2007**, *38*, 35.
(17) Li, Q. Y.; Du, J. H.; Xi, Z. P. *Trans. Nonferrous Met. Soc. China* **2007**, *17*, s560.
(18) Abdelkader, A. M.; El-Kashif, E. *ISIJ Int.* **2007**, *47*, 25.
(19) Okabe, T. H.; Park, I.; Jacob, K. T.; Waseda, Y. *J. Alloys Compd.* **1999**, *288*, 200.
(20) Okabe, T. H.; Oda, T.; Mitsuda, Y. *J. Alloy. Compd.* **2004**, *364*, 156.
(21) Chen, G. Z.; Fray, D. J.; Farthing, T. W. *Nature* **2000**, *407*, 361.
(22) Chen, G. Z.; Fray, D. J.; Farthing, T. W. *Metall. Mater. Trans. B* **2001**, *32*, 1041.
(23) Chen, G. Z.; Fray, D. J. *J. Electrochem. Soc.* **2002**, *149*, E455.
(24) Jin, X. B.; Gao, P.; Wang, D. H.; Hu, X. H.; Chen, G. Z. *Angew. Chem., Int. Ed.* **2004**, *43*, 733.
(25) Yan, X. Y.; Fray, D. J. *Adv. Funct. Mater.* **2005**, *15*, 1757.
(26) Chen, G. Z.; Gordo, E.; Fray, D. J. *Metall. Mater. Trans. B* **2004**, *35*, 223.
(27) Wu, T.; Xiao, W.; Jin, X.; Liu, C.; Wang, D. H.; Chen, G. Z. *Phys. Chem. Chem. Phys.* **2008**, *10*, 1809.
(28) Wang, D. H.; Qiu, G. H.; Jin, X. B.; Chen, G. Z. *Angew. Chem., Int. Ed.* **2006**, *45*, 2384.
(29) Ma, M.; Wang, D. H.; Wang, W. G.; Hu, X. H.; Jin, X. B.; Chen, G. Z. *J. Alloys Compd.* **2006**, *420*, 37.
(30) Nohira, T.; Yasuda, K.; Ito, Y. *Nat. Mater.* **2003**, *2*, 397.
(31) Yasuda, K.; Nohira, T.; Hagiwara, R.; et al. *Electrochim. Acta* **2007**, *53*, 106.
(32) Sakamura, Y.; Kurata, M.; Inoue, T. *J. Electrochem. Soc.* **2006**, *153*, D31.
(33) Iizuka, M.; Sakamura, Y.; Inoue, T. *J. Nucl. Mater.* **2006**, *359*, 102.
(34) Sakamura, Y.; Omori, T.; Inoue, T. *Nucl. Technol.* **2008**, *162*, 169.

10.1021/cm802237v CCC: $40.75
Published on Web 11/11/2008

oxide is reduced to the metal or alloy with the oxygen being ionized into the molten salt and then discharged at the anode. The temperature is usually not higher than 950 °C and the cell voltage below the decomposition voltage of the molten salt.

Of particular relevance to this work is that, although not well described, in all previous successful experiments, the metallised cathode always possessed the same shape as the oxide precursor (e.g., cylindrical pellets).[15,29] This common observation suggests a possibility to manufacture the oxide precursor into a desired engineering shape that can be directly electro-reduced to the metallic artifact.[35] Such a process, if feasible, would be simple, fast, and low in energy consumption, promising new manufacturing applications. Nevertheless, there remains a concern. Could such produced metal be satisfactorily consolidated?

Herein, we report unprecedented results from cyclic voltammetry of the ZrO_2 powder and potentiostatic electrolysis (three-electrode cell) of porous ZrO_2 pellets in molten $CaCl_2$. The electrochemistry is correlated with scanning electron microscopy (SEM), energy-dispersive X-ray spectroscopy (EDX) and X-ray diffraction spectroscopy (XRD) to elaborate the electro-reduction mechanism. Also, new evidence is presented for electro-deoxygenation induced in situ sintering or consolidation in the metallized products. More importantly, we demonstrate for the first time the feasibility of direct electro-fabrication of consolidated Zr metal and Zr−2.5Nb alloy tubes from the oxide precursors by constant voltage (two-electrode cell) electrolysis in molten $CaCl_2$.

Experimental Section

Metallic Cavity Electrode (MCE). The MCE was previously demonstrated.[36] Figure 1 shows the cyclic voltammogram (CV) and scanning electron microscopic (SEM) images of the MCE used in this work. It was fabricated by high-speed mechanical drilling two ~0.5 mm circular holes through a molybdenum (Mo) foil (0.5 mm thickness, ~1.5 mm width, ~120 mm length, 99.9% purity). The foil was then polished on metallographic sandpaper, boiled in concentrated NaOH for 30 min to dissolve any oxide layer, washed in distilled water and acetone, and dried in air.

Oxide Tubular Precursors. Oxide tubular precursors were prepared by slip-casting the aqueous slurry of the ZrO_2 powder (≥99.0%, 0.5−1 μm, Sinopharm Chemical Reagent Co. Ltd., China) or its mixture with another oxide powder (e.g., 2.68 wt % Nb_2O_5 and 97.32 wt % ZrO_2, for the Zr−2.5Nb Zircaloy) in a mold of Plaster of Paris. Following drying (50−60 °C, 2−3 h) and sintering (1000 °C, 4 h) in air, tubular oxide precursors were fabricated in various dimensions (0.8−4.0 cm length, 0.8−1.8 cm external diameter and 0.2−0.4 cm wall thickness) so that they could be fit into the electrolytic cells of this work. The precursors were also prepared by die-pressing the powder into a cylinder that was sintered and drilled with a central hole.

Cyclic Voltammetry and Chronoamperometry (Potentiostatic Electrolysis) Using the MCE. These were performed in a three-electrode cell using the MCE filled with the ZrO_2 powder (~0.5 mg in the two holes) as a working electrode. The powder was manually filled into the cavity by repetitively pressing the powder against a glass slide.[28,36] Electrochemical control was achieved by a computer assisted CHI660 electrochemical system (Shanghai Chenhua Instrument Co. Ltd., China). The counter electrode was a small graphite crucible containing 35−40 g of molten $CaCl_2$ prepared by thermal dehydration of $CaCl_2 \cdot 2H_2O$ (ACS grade, Shanghai Bioengineering Co. Ltd.). The reference was a quartz-sealed Ag/AgCl electrode.[37] It is worth mentioning that the AgCl in the chloride melt sealed in the quartz tube may dissociate into the Ag^+ and Cl^- ions, but these ions would be likely in complexed forms. This means that the potential of a silver/silver salt reference will be affected by the anion of the silver salt. Thus, the expression of Ag/AgCl is used in this paper to reflect that it was AgCl, instead of e.g. AgF or $AgNO_3$, that was used in the reference, although Ag/AgCl (10 mol %) or Ag/Ag(I) may be similarly appropriate expressions.

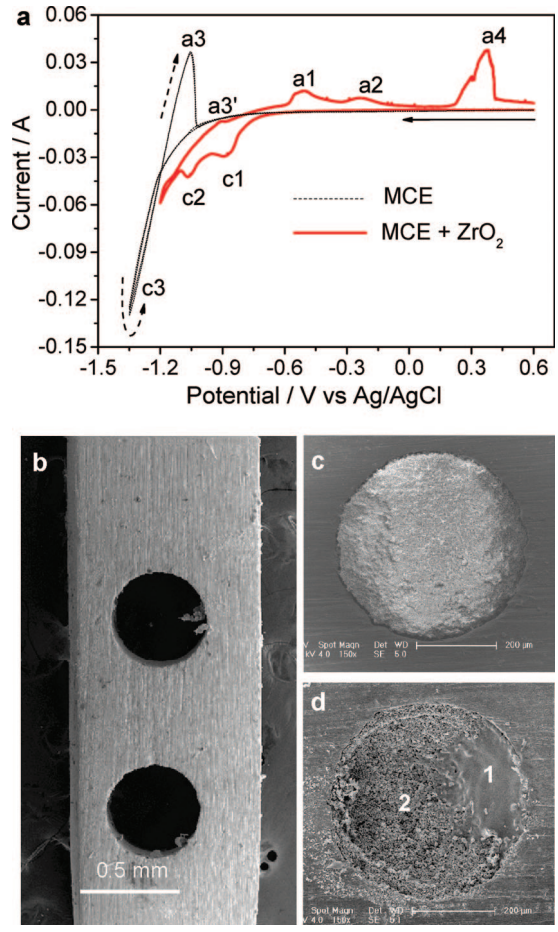

Figure 1. (a) Cyclic voltammograms of a two-hole molybdenum cavity electrode (MCE) with (solid red line) and without (dashed black line) being filled with the ZrO_2 powder in molten $CaCl_2$ at 850 °C Scan rate: 20mV/s. (b−d) SEM images of the MCE (b) without and with filled ZrO_2 powder (coated with Au) (c) before and (d) after potentiostatic electrolysis at −0.90 V and 850 °C for 1000 s. EDX analyses of the marked regions in d revealed 14.5 at % O in **1** and 43.1 at % O in 2. (The oxygen content in fully oxygenated Zr metal and ZrO_2 are respectively 28.5[39] and 66.7 at %.)

Potentiostatic Electrolysis of the Porous ZrO_2 Pellet in the Three-Electrode Cell. The ZrO_2 powder (~1.0 g) was pressed into cylindrical pellets under 4−6 MPa. After sintering in air at 950 ± 50 °C for 2 h, the pellet slightly shrank to ~19.0 mm diameter and ~1.0 mm thickness. The porosity was estimated to be 40−50% on

(35) Fray, D. J.; Chen, Z.; Farthing, T. W. European Patent EP1333110, 2003.
(36) Qiu, G. H.; Ma, M.; Wang, D. H.; Jin, X. B.; Hu, X. H.; Chen, G. Z. *J. Electrochem. Soc.* **2005**, *152*, E328.
(37) Gao, P.; Jin, X. B.; Wang, D. H.; Hu, X. H.; Chen, G. Z. *J. Electroanal. Chem.* **2005**, *579*, 321.

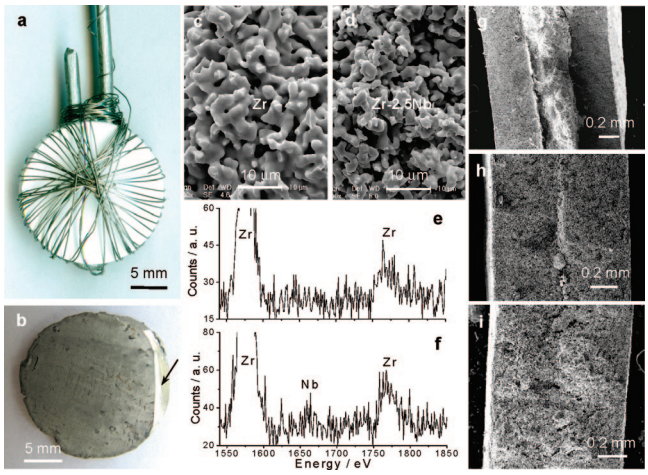

Figure 2. (a, b) Photographs of (a) a ZrO_2 pellet (~1.5 g, 1.7 mm thick) assembled into a cathode with molybdenum wires and (b) its appearance after electrolysis in molten $CaCl_2$ at 850 °C and 3.0 V for 10 h. The shining edge as indicated by the arrow in b was a result of grinding against the sandpaper. (c−f) SEM images and EDX spectra (high binding energy data only) of the electrolyzed pellets of (c, e) ZrO_2 and (d, f) 2.68 wt % Nb_2O_5 and 97.32 wt % ZrO_2 (for the Zr−2.5Nb alloy). (g−i) SEM images of the cross-sections of three ZrO_2 pellets electrolyzed at 900 °C with different electrolysis voltages and times: (g) 3.2 V, 2 h (XRD and EDX confirmed the central layer to be mixed Zr metal and perovskite and the outer layers the Zr metal), (h) 3.3 V, 3 h (the central layer just disappeared), and (i) 3.2 V, 4 h (uniform internal structure). Note that the overall pellet thickness decreases from g to i, resulting from more sintering with further electroreduction.

the basis of the pellet's mass and volume, and the density of ZrO_2. The sintered pellet was wrapped with Mo wires to assemble the working electrode (see Figure 2a). A graphite rod counter electrode and the quartz-sealed Ag/AgC reference electrode were applied to maintain the potential of the oxide pellet electrode.[38]

A sealable stainless steel tube reactor was used for the electrolysis of the pellet. About 1000 g anhydrous $CaCl_2$ (AR grade, Shanghai Silian Chemicals) was contained in a large graphite crucible, and dried in the reactor for more than 48 h at 200−300 °C in air. Subsequently, the reactor was sealed and continuously flushed with argon (>99.999%) when the temperature was raised to and maintained at 500−700 °C for 5 h, and finally to the working temperature (850−950 °C).

Pre-electrolysis was performed at 2.6 V between a nickel sheet cathode and the graphite rod anode for a sufficiently long time (>2 h) to further remove residual water and some redox active impurities from the molten salt. During electrolysis, the effluent gas from the reactor was guided into a buffering bottle filled with anhydrous $CaCl_2$ granules, a flask filled with concentrated H_2SO_4, and then through a solution of 0.1 M NaOH before escaping into a fume hood. The electrolysis was controlled by a high-accuracy four-electrode battery testing system (Shenzhen Neware Electronic Ltd., China) linked to a PC computer.

Constant Voltage Electrolysis of the Porous ZrO_2 Pellet in a Two-Electrode Cell. These experiments were done on slightly thicker porous ZrO_2 pellets (19.0 mm diameter, 1.6−1.7 mm thickness, and ~1.5 g weight) prepared in the same way as described above. The electrolysis was performed between the assembled pellet cathode and the graphite rod anode under constant voltage control (i.e., without using the reference electrode). Other conditions were the same as mentioned above for the potentiostatic electrolysis.

In this work, the resistance of the two-electrode cell measured at 850 °C by the ac impedance method was typically ~0.5 ohm, and the dc background current at 3.0 V was ~0.5 A. Thus, the minimum ohmic voltage loss (= current × resistance) would be 0.25 V and the maximum electrolysis voltage applied in this work was thus 3.3 V to avoid decomposition of the molten salt.

Characterizations of Samples. After experiments in molten salts, the sample was lifted into a cooling argon stream, washed in distilled water and dried in a vacuum. It was then examined by scanning electron microscopy (SEM) (FEI Sirion field emission gun SEM, or KYKY-EM3200 digital SEM, Beijing), energy-dispersive X-ray analysis (EDX) (EDAX GENESIS 7000), powder X-ray diffraction spectroscopy (XRD) (Shimadzu X-ray 6000 with Cu Kα1 radiation at λ =1.5405Å), inductively coupled plasma atomic absorption spectroscopy (ICP-AAS) (Agilent 7200a Japan), and inert gas fusion-infrared absorption oxygen analysis (RO-416DR, LECO, USA).

Results and Discussion

Figure 1a shows a typical cyclic voltammogram (CV) of the fine ZrO_2 powder (particle sizes, 0.5−1 μm; mass, ~0.5 mg) in molten $CaCl_2$ at 850 °C, using a previously reported metallic cavity electrode (MCE)[36] as the working electrode, and Ag/AgCl reference[37] and graphite counter electrodes. Images b and c in Figure 1 show an MCE before and after being filled with the ZrO_2 powder. On the CV of the ZrO_2-MCE, the reduction starts slightly after −0.70 V, followed by two reduction peaks at −0.90 V (**c1**) and −1.07 V (**c2**). Upon reversing the potential sweep, three oxidation peaks were recorded, i.e., **a1** (−0.50 V), **a2** (−0.22 V),and **a4** (0.37 V). These current peaks are absent on the CV of the empty MCE and hence clearly belong to the electrochemistry of ZrO_2. Potentiostatic electrolysis of the ZrO_2-MCE at **c1** and **c2** for about 10−15 min and analysis of the products by EDX revealed either Zr and O (**c1**) or Zr alone (**c2**), but no Ca or Cl. Considering the presence of various solid oxygen solution (up to 35 at % O) and the metallic pseudo-oxide phases (Zr_xO, $x \geq 2$) in the O−Zr binary phase diagram,[22,39] the following reactions may be associated with the two reduction peaks.

$$xZrO_2 + 2(2x-1)e \rightleftharpoons Zr_xO + (2x-1)O^{2-} \quad \textbf{(c1)} \tag{1}$$

$$Zr_xO + 2e \rightleftharpoons xZr + O^{2-} \quad \textbf{(c2)} \tag{2}$$

It is worth mentioning that previous investigations on the electroreduction of some metal oxides in molten $CaCl_2$ demonstrated the formation of various perovskites as the intermediate products.[16−18,36,40−43] Simply immersing a porous pellet of the ZrO_2 powder (see Figure 2a) in pure molten $CaCl_2$ at 850 °C for 12 h led to no change in the pellet as confirmed by visual observation and XRD analysis. However, repeating the experiment in CaO saturated molten $CaCl_2$, the perovskite phase was detected on the outer layer of the pellet by XRD and EDX, suggesting the following reaction.

(38) Xiao, W.; Jin, X. B.; Deng, Y.; Wang, D. H.; Hu, X. H.; Chen, G. Z. *ChemPhysChem* **2006**, *7*, 1750.
(39) Arroyave, R.; Kaufman, L.; Eagar, T. W. *Calphad* **2002**, *26*, 95.
(40) Dring, K.; Dashwood, R.; Inman, D. *J. Electrochem. Soc.* **2005**, *152*, D184.
(41) Schwandt, C.; Fray, D. J. *Electrochim. Acta* **2005**, *51*, 66.
(42) Jiang, K.; Hu, X. H.; Ma, M.; Wang, D. H.; Qiu, G. H.; Jin, X. B.; Chen, G. Z. *Angew. Chem., Int. Ed.* **2006**, *45*, 428.
(43) Gordo, E.; Chen, G. Z.; Fray, D. J. *Electrochim. Acta* **2004**, *49*, 2195.

$$ZrO_2 + CaO \rightleftharpoons CaZrO_3 \quad \Delta G^o\,(850\ ^\circ C) = -35.2\ kJ \tag{3}$$

(It should be noted that, in molten $CaCl_2$, CaO is likely dissociated into Ca^{2+} and O^{2-} ions that were approximated by liquid CaO in the literature.[40]) The perovskite phase is not always stoichiometric and can have the general formula of $Ca_\alpha ZrO_\beta$ ($\alpha \leq 1$ and $2 < \beta \leq 3$)). Apparently, because Reaction (3) has only a moderate change in the Gibbs free energy and involves the conversion between two solid phases (ZrO_2 and $CaZrO_3$), it may not be very fast. Thus, for the small amount of ZrO_2 powder used in the MCE, the reduction could be too fast to show clearly the occurrence of Reaction (3). It is worth mentioning that previous potentiostatic electrolysis of similarly prepared Cr_2O_3-MCE also found no Ca in the product, but various $Ca_\alpha CrO_\beta$ phases were detected in electrolysis of larger porous Cr_2O_3 pellets.[26,43]

To study the mass and time effects on Reaction (3), potentiostatic electrolysis was performed on porous ZrO_2 pellets (~1 mm thickness and 1.0 g weight) in the potential ranges of **c1** and **c2** for 10−12 h. Figure 3a compares the XRD patterns of the electrolysis products obtained at four different potentials: −0.70 V (before the onset of **c1**), −0.90 V (at **c1**), −1.00 V (after **c1** but before **c2**), and −1.10 V (after **c2**). It can be seen that no change occurred at −0.70 V. However, the electrolysis at −0.90 V for 12 h and at −1.00 V for 10 h produced both Zr metal and perovskite. Complete reduction to the Zr metal occurred at −1.10 V. These findings suggest that the following general reactions could have occurred during the electro-reduction of the porous ZrO_2 pellet.

$$ZrO_2 + \alpha Ca^{2+} + (4 - 2\beta + 2\alpha)e \rightleftharpoons Ca_\alpha ZrO_\beta + (2 - \beta)O^{2-} \tag{4}$$

$$Ca_\alpha ZrO_\beta + 2(\beta - \alpha)e \rightleftharpoons Zr + \beta O^{2-} + \alpha Ca^{2+} \tag{5}$$

$$xCa_\alpha ZrO_\beta + 2x(\beta - \alpha - 1)e \rightleftharpoons Zr_xO + (\beta x - 1)O^{2-} + \alpha x Ca^{2+} \tag{5a}$$

$$Zr_xO + 2e \rightleftharpoons xZr + O^{2-} \tag{5b}$$

Note that reaction 4 is equivalent to reaction 3 for $\alpha = 1$ and $\beta = 3$, and has the same form as the intercalation reaction for $\beta = 2$; i.e., it brings Ca^{2+} into the solid phase without removal of oxygen.[26,36,42] Clearly, other reaction equations of thermodynamic equivalence may be derived from reactions 1−5. For example, the sums of (1) + (3) = (6a) and [(1) + (2)]/x + (3) = (6b) or (6c) agree well with the XRD detection of both of the Zr_xO (or Zr metal) and perovskite phases in partially reduced pellets (see Figure 3a).

$$(x+1)ZrO_2 + CaO + 4xe \rightleftharpoons Zr_xO + CaZrO_3 + (2x - 1)O^{2-} \tag{6a}$$

$$2ZrO_2 + CaO + 4e \rightleftharpoons Zr + CaZrO_3 + 2O^{2-} \tag{6b}$$

$$2ZrO_2 + Ca^{2+} + 4e \rightleftharpoons Zr + CaZrO_3 + O^{2-} \tag{6c}$$

Reaction 6c is derived from reaction 6b, assuming CaO is completely dissociated into the Ca^{2+} and O^{2-} ions in the molten salt.

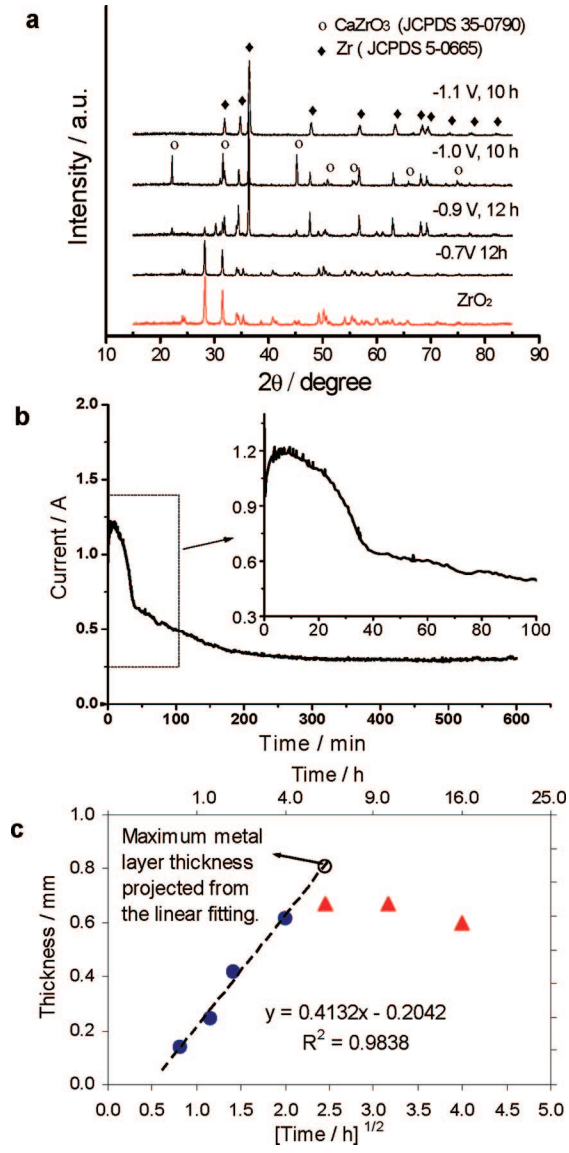

Figure 3. (a) Powder XRD patterns of ZrO_2 and the products from potentiostatic electrolysis (three-electrode cell) of ZrO_2 pellets (~1.0 mm thickness, ~19.0 mm diameter, ~1.0 g weight) under the indicated conditions. (b) A typical current−time plot recorded during constant voltage electrolysis (two-electrode cell) of the ZrO_2 pellet (1.6−1.7 mm thickness, ~19.0 mm diameter, ~1.5 g) at 3.0 V. The inset is the expanded boxed portion of the plot. (c) The correlation between the thickness of the metallised surface layer (as shown in Figure 2g) and the time of electrolysis at 3.0 V. The dashed line and the equations in (c) are the results of linear fitting according to the parabolic law (thickness vs time$^{1/2}$). The molten salt temperature was 850 °C in all these experiments.

The three-electrode cell used in above-mentioned experiments is advantageous in fundamental studies but the simpler two-electrode cell is preferred in the industry. Therefore, constant-voltage electrolysis was performed using the porous ZrO_2 pellet cathode (1.6−1.7 mm thickness, see Figure 2a) and a graphite anode to identify the electrolysis conditions in the two-electrode cell. In such experiments, the cell voltage was investigated below the decomposition voltage of $CaCl_2$ which is theoretically 3.245 V at 850 °C, but should be experimentally higher than 3.3 V considering the ohmic voltage loss due to the resistance largely from the electrolyte and electrodes.

Figure 2b displays an electroreduced ZrO_2 pellet in molten $CaCl_2$ at 3.0 V and 850 °C for 10 h. Grinding any part of

the pellet surface on the sandpaper resulted in the metallic luster (see the arrow indicated shining edge in the photograph). The SEM image in Figure 2c was taken from the interior of the reduced pellet, showing interconnected 5−10 μm nodular particles similar to those in similarly prepared Ti metal.[21−23,29,42] The electrolysis was also extended to pellets of mixed ZrO_2 and other oxide powders under similar conditions. Figure 2d is the SEM image of the interior of an electrolyzed pellet of mixed Nb_2O_5 (2.68 wt %) and ZrO_2 (97.32 wt %) powders with the composition being in agreement with the Zr−2.5Nb Zircaloy.

The EDX spectrum (Figure 2e) and XRD pattern (almost identical to the top one in Figure 3a) proved the electrolyzed pellet in Figure 2b to be pure Zr metal. In this particular sample, the oxygen content was about 2700 ppm as measured by the inert gas fusion-IR absorption oxygen analyzer (LECO). The EDX analysis (Figure 2f) over the image in Figure 2d revealed the presence of Nb although the signal was fairly weak. The Nb content in the alloy was further confirmed to be 2.51 wt % by inductively coupled plasma atomic absorption spectrometry (ICP-AAS).

In both three- and two-electrode electrolysis experiments, the recorded current−time ($I-t$) plots exhibited very similar features under comparable cathode potential and cell voltage. A typical $I-t$ plot from the constant voltage electrolysis of ZrO_2 pellets is presented in Figure 3b. It features an initial current peak over a short period (see the inset) and then a longer declining tail which ends at the same level as the background current (as measured in the absence of ZrO_2).

Removing the pellet from the molten salt at different times along the $I-t$ plot revealed sandwiched and uniform structures in partially and fully reduced pellets, respectively, as shown in Figure 2g−i. XRD and EDX analyses proved the outer layer in Figure 2g to be the Zr metal (with dissolved oxygen), but the core to be a mixture of Zr metal and perovskite. Measuring the thickness of the outer metallic layer led to plots like that in Figure 3c. The pellets in h and i in Figure 2 were fully metallized. These findings agree in general with the reduction taking place at the metal/oxide/electrolyte three-phase interlines (3PIs) that expanded along the oxide pellet's surface first (the initial period before the linear region in Figure 3c), leading to the current peak on the $I-t$ plot, and then propagated into the pellet at a decreasing rate and hence the declining current tail at later times of the electrolysis. The latter is dominated by mass transfer through the pores of the metallic layer and corresponds to the linear region in Figure 3c in accordance with the parabolic law.[29,44]

However, it can be seen in Figure 3c that the metal layer thickness at the maximum point (0.67 mm at 6 h) and later electrolysis times (e.g., 0.60 mm at 16 h) is far smaller than a half of the oxide pellet thickness (1.6−1.7 mm). The data in Figure 3c were obtained from electrolysis at 850 °C and 3.0 V. At higher cell temperatures and voltages, the time for the electrolysis to reach completion became shorter. For example, at 900 °C and 3.2 V, electrolysis for just 4 h led to complete reduction. The overall thickness of the metallised pellets shown in h and i in Figure 2 was, respectively, 1.05 and 0.93 mm. These observations are strong evidence of the metal particles in the fully reduced pellets being significantly sintered together. It is interesting to note that Figure 3c shows a projected maximum metal layer thickness (0.808 mm) according to the parabolic law. This extrapolated value is very close to a half of the oxide pellet thickness, suggesting the sintering occurred mostly after the full metallisation of the oxide pellet when the electrode reaction was mostly electro-deoxygenation,[21−23] i.e., the removal of dissolved oxygen from the metal.

Table 1. Typical Results from Electrolysis of ZrO_2 Pellets

	electrolysis conditions				
	850 °C,[a] 3.0 V, 10 h	900 °C,[a] 3.1 V, 4 h	900 °C,[a] 3.1 V, 14 h	950 °C,[a] 3.0 V, 10 h	850 °C,[b] 3.0 V, 6 h
C.E. (%)	35.4	28.1	24.3	12.8	45.0
E.C. (kWh/kg-Zr)	10.5	12.98	15.0	27.42	7.8
O content (ppm)	2700	2000	1200	1100	1800

[a] Two-electrode graphite cell and constant voltage in molten $CaCl_2$. [b] Using a titanium crucible for electrolysis under the same conditions.

Comparing the mass change of the cathode (pellet) before and after electrolysis, it was found that the Zr recovery yield could reach at 99%, which is high but expected because the electro-reduction proceeded from the solid oxide to the solid metal. The current efficiency (C.E.) and energy consumption (E.C.) of the electrolysis can be derived from the current−time plots. These parameters depend on the oxygen content in the product. As shown in Table 1, the oxygen level decreased in general with increasing the cell voltage and temperature, and the electrolysis time. However, such variations led to lower C.E. and higher E.C. values.

We would like to highlight that the electrometallized ZrO_2 pellets retained very well the geometry of the oxide precursor as shown in a and b in Figure 2. In addition, it was found that as long as the pellet thickness was not greater than 2 mm, complete electroreduction of ∼1.5 g of ZrO_2 could be achieved in 3−4 h at 900−950 °C and 3.0−3.3 V. Particularly, under these conditions, the metallized pellet underwent significant sintering although the molten salt temperatures were much lower than the melting point of pure Zr metal (850−950 °C vs 1855 °C).

Besides temperature and time, the packing density and the oxygen content of the powder could also influence the degree of sintering. The SEM image in Figure 1d was taken from the ZrO_2-MCE after potentiostatic electrolysis for 1000 s at a potential of −0.90 V, showing a sintered region (**1**) next to the edge of the cavity. The EDX detected oxygen contents in the sintered (**1**) and unsintered (**2**) areas were 14.5 at. % (∼3 wt %) and 43.1 at % (11.7 wt %), respectively. Although not high in accuracy, the EDX results indicate qualitatively that a lower oxygen content is more favorable for the sintering process. It should be pointed out that the phenomenon shown in Figure 1d is not very common among MCE experiments, and it is not yet clear whether there was additional influence from the packing density variation between the MCE experiments in which the powder was manually packed into the MCE.

However, in the ZrO_2 pellet electrolysis experiments, packing density must be fairly consistent because all pellets

(44) Deng, Y.; Wang, D. H.; Xiao, W.; Jin, X. B.; Hu, X. H.; Chen, G. Z. *J. Phys. Chem. B* **2005**, *109*, 14043.

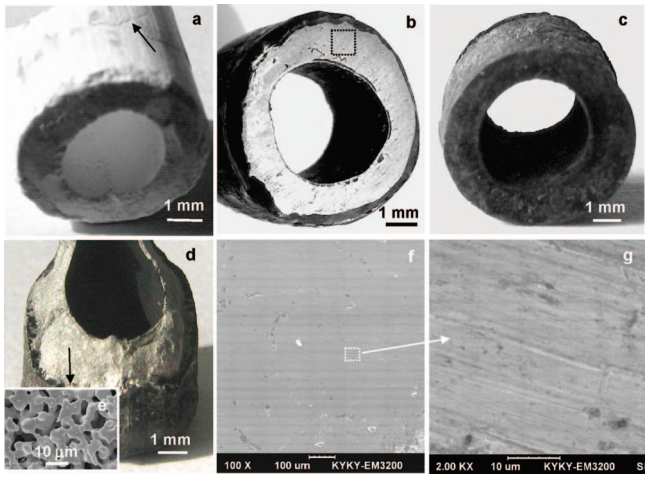

Figure 4. (a, b) Photographs of a slip-cast and sintered tubular precursor of ZrO_2 before (a) and after (b) complete electro-reduction in molten $CaCl_2$ (see the text for more detail). The shining metallic end of the Zr tube was a result from grinding on the sandpaper. (c) A similarly prepared Zr−2.5Nb tube. (d) A broken section of the Zr tube in b produced by a hammer hit. The fracture is believed to have resulted from an original crack in the oxide precursor similar to that indicated by the arrow in a. (e) SEM image obtained from the surface of the broken section in d. (f, g) SEM images of the boxed region in the polished tube end in b at different magnifications.

were of very comparable weights and prepared using the same procedure and conditions. Therefore, in these cases, the oxygen content should be an important factor. Indeed, most electrolyzed pellets with a relatively low oxygen content were seriously sintered and manually unbreakable. The oxygen content in the product decreases with increasing the electrolysis voltage and/or time as shown in Table 1. The effect of electrolysis time on sintering is also supported by the plot in Figure 3c which shows clearly that the sintering proceeded in the metallised pellet when electrodeoxygenation went further with increasing the electrolysis time.

As mentioned before, the mostly used form of the Zr metal (Zircaloy) is the fuel cladding tubes in nuclear reactors. These tubes are usually less than 1.0 mm in wall thickness and 8−15 mm in inner or outer diameter, although the length varies with reactor designs.[6,7] The capability of the electroreduction process to retain the oxide precursor shape and to sinter in situ the metallic product promises direct electrochemical fabrication of the cladding tubes at a lower cost. It was then decided to fabricate small tubular precursors with or without a closed end using the ZrO_2 powder or its mixture with Nb_2O_5. These tubular oxide precursors were comparable to the cladding tubes in diameter and wall thickness, and had such a length that they could be placed into the electrolytic cells used in this work. Various electrolysis conditions were tested, including changing the crucible material from graphite to titanium (to reduce carbon contamination to the product) and varying the cell voltage between 2.6 and 3.1 V, the temperature between 850 and 900 °C, and the time between 24 and 48 h (to balance reduction and sintering). The purpose was to not only fully electro-reduce the porous oxide precursor, but also to consolidate the obtained metal as much as possible via the electro-deoxygenation assisted in situ sintering.

A successful example is displayed in a and b in Figure 4 with the 48 h electrolysis being performed in a titanium crucible[21−23] and finished at 900 °C and 3.1 V. Note that apart from the shrinkage in comparison with the oxide precursor, the electrolytic Zr tubes became readily lustrous by polishing on the sandpaper, which was responsible for the shining metallic end of the Zr tube in Figure 4b. A similarly prepared Zr−2.5Nb tube is shown in Figure 4c. The electrolytic Zr tube was very strong to manual handling, but could be broken by hammer hitting. The surface of the broken section was silvery, see Figure 4d, and possessed a spongelike microstructure as shown in Figure 4e. It was later realized that, in the case of d and e in Figure 4, the fracture was related to an original crack in the oxide precursor as indicated by the arrow in Figure 4a. This means that the electroreduction along the surface of the broken section in Figure 4d was more like that along the external surfaces of the oxide tube. On the other hand, when the polished Zr-tube end in Figure 4b was examined under the SEM, almost fully densified pictures were seen in the central regions of the wall, see f and g in Figure 4, although the outer and inner surfaces of the tube were also spongelike, similar to but slightly denser than that shown in Figure 2c. The cause for the less sintered surface regions is not yet known, but could be related to the molten salt near the surface having a greater moving freedom (convection) than that inside the pores of the walls.

Interestingly, it was found that a fully electrometallized Zr-tube with a closed end did not allow water to pass, suggesting the pores as shown in Figures 2c and 4e to be likely blocked. Although this finding is further evidence of the fully electroreduced samples being well-consolidated, more detailed investigation is necessary to verify the presence or absence of any closed pores in the metal that may have inclusions of solidified salt. It is, however, worth noting some recent reports of direct evidence of the absence of solidified salt in either open[28] or closed[50] pores in fully metallized products from the electroreduction process. In this work, Ca was always undetectable in well electroreduced and sintered samples by EDX, which has an analysis depth of a few micrometers beneath the sample's surface. Thus, it seems to be unlikely for solidified salt to be inside the metal even if closed pores may be present. An experimentally supported explanation is the molten salt being nonwetting to the almost oxygen-free metal surface.[28,51] This means that the molten salt could be expelled by the capillary force when the macropores shrink to micro- and nanopores with continuous electrodeoxygenation and in situ sintering.

Conclusions

In conclusion, we have demonstrated the facile electroreduction of porous thin pellets (<2 mm thickness) of ZrO_2 or its mixture with Nb_2O_5 in molten $CaCl_2$ at 850−950 °C to fully metallized and well-sintered Zr metal or Zr−2.5Nb alloy pellets with very low oxygen content (achieved 1100 ppm). The energy consumption can be as low as 7.8 kWh/(kg of Zr). (The energy consumptions of the Kroll process for the extraction of Ti and Zr are, respectively, 45−55 kWh/(kg of Ti) and 25−30 kWh/(kg

of Zr), assuming the same process efficiency.[42,45]) More importantly, the process can be applied for electrochemical fabrication of well-consolidated tubular artifacts of pure Zr metal and the Zr−2.5Nb alloy directly from the oxide precursors. Although such metal tubes with porous surfaces may find applications in chemical processes and medical treatments,[46−49] the finding of the almost fully densified central part of the metal tube walls promises electrochemical fabrication of near-shape nonporous Zircaloy cladding tubes for nuclear reactors in future work.

Acknowledgment. The authors acknowledge the financial support from the NSFC and the EPSRC (Grants 20573081, 20773094, EP/F026412/1), and the National Basic Research Program of China (2007CB613800).

CM802237V

(45) Yan, D. *Energy Saving Non-ferrous Metall.* **2004**, *21*, 12, in Chinese.
(46) Vianin, L.; Comninellis, Ch. *Electrochim. Acta* **1998**, *43*, 1109.
(47) Nagakura, M. Japanese Patent JP2002212573, 2002.
(48) Davidson, J. A.; Tuneberg, L. H. PCT Patent WO0068448, 2000.
(49) Oliveira, N. T. C.; Biaggio, S. R.; Rocha-Filho, R. C.; Bocchi, N. *J. Biomed. Mater. Res., A* **2005**, *74A*, 397.
(50) Chen, G. Z.; Fray, D. J. *Miner. Process. Extr. Metall. (Trans. Inst. Min Metall. C)* **2006**, *115*, 49.
(51) Chen, G. Z.; Fray, D. J. *Light Met.* **2004**, 881.